

GS-Net: Generalizable Plug-and-Play 3D Gaussian Splatting Module

Yichen Zhang^{1,2,3,†}, Zihan Wang^{1,2,3,†}, Jiali Han⁴, Peilin Li³, Jiaxun Zhang^{1,2,5}, Jianqiang Wang^{1,2}
Lei He^{1,2,*} and Keqiang Li^{1,2}

Abstract—3D Gaussian Splatting (3DGS) integrates the strengths of primitive-based representations and volumetric rendering techniques, enabling real-time, high-quality rendering. However, 3DGS models typically overfit to single-scene training and are highly sensitive to the initialization of Gaussian ellipsoids, heuristically derived from Structure from Motion (SfM) point clouds, which limits both generalization and practicality. To address these limitations, we propose GS-Net, a generalizable, plug-and-play 3DGS module that densifies Gaussian ellipsoids from sparse SfM point clouds, enhancing geometric structure representation. To the best of our knowledge, GS-Net is the first plug-and-play 3DGS module with cross-scene generalization capabilities. Additionally, we introduce the CARLA-NVS dataset, which incorporates additional camera viewpoints to thoroughly evaluate reconstruction and rendering quality. Extensive experiments demonstrate that applying GS-Net to 3DGS yields a PSNR improvement of 2.08 dB for conventional viewpoints and 1.86 dB for novel viewpoints, confirming the method’s effectiveness and robustness.

I. INTRODUCTION

Photo-realistic and real-time 3D scene rendering has long been a significant and challenging task in computer vision, with wide applications in areas such as autonomous driving [13]. In recent years, Neural Radiance Fields (NeRF) [12, 28] have made remarkable progress in this field, achieving high-fidelity rendering without explicitly modeling 3D scenes, textures, or lighting. However, NeRF’s stochastic sampling and volumetric rendering are computationally intensive, severely impacting its performance and leading to slow rendering speeds. To address the need for real-time neural rendering, the 3D Gaussian Splatting (3DGS) method was introduced, representing scenes through Gaussian ellipsoids and utilizing fast rasterization to produce high-quality images.

However, 3DGS[2] typically handles only single scenes, and initializes Gaussian ellipsoid parameters from sparse yet geometrically accurate point clouds via Structure from Motion (SfM)[15], followed by iterative optimization and density control using photometric loss functions. This approach requires separate models for each scene, lacking cross-scene generalization. Additionally, 3DGS is sensitive to the heuristic initialization of Gaussian ellipsoids from

SfM point clouds. If the sparse point clouds fail to capture scene details, this dependence hinders further optimization and limits practical applicability.

To address these challenges, we propose GS-Net, a generalizable plug-and-play 3DGS module. This module uses sparse point clouds as input to generate denser Gaussian ellipsoids, allowing training and testing across different scenes, overcoming the scene-boundary limitations of traditional 3DGS. As a plug-and-play module, GS-Net offers practicality and compatibility, making it suitable for all 3DGS frameworks. To comprehensively evaluate GS-Net’s performance in autonomous driving scenarios, we created the CARLA-NVS dataset, supporting training and evaluation from 12 camera viewpoints. Experiments show significant improvements in rendering quality with GS-Net.

Our main contributions are as follows:

- 1) We propose GS-Net, a generalizable plug-and-play 3DGS module designed to generate dense initial Gaussian ellipsoids and parameters from sparse SfM point clouds. To the best of our knowledge, this is the first network to directly learn Gaussian ellipsoids from sparse point clouds.
- 2) GS-Net offers strong practicality and compatibility as a plug-and-play module, applicable to 3DGS frameworks and their derivative models.
- 3) We have developed the CARLA-NVS dataset, which is the first to provide 12 dense-view images, enabling comprehensive evaluation of scene reconstruction and rendering quality, as well as supporting autonomous driving perception tasks.

II. RELATED WORK

A. Densification Strategies in 3DGS

3D Gaussian Splatting (3DGS) [1, 2, 28] utilizes anisotropic Gaussian functions and rasterization techniques to achieve real-time 3D scene reconstruction. To generate high-quality ellipsoids, 3DGS introduces density control strategies. However, the process is unstable and may cause artifacts. To solve the problem, researchers have proposed various methods. GaussianPro [27] introduces a progressive propagation strategy during optimization to generate new Gaussian ellipsoids. This method employs plane constraints to effectively propagate depth and normal information on textureless regions. Additionally, FSGS [8] generates new Gaussian ellipsoids by combining neighborhood distances between points and integrating monocular depth cues to guide the densification process. Meanwhile, SemGauss-SLAM [14]

This work is supported by National Natural Science Foundation of China, Science Fund for Creative Research Groups (Grant No.52221005)

[†]These authors contributed equally to this work.

¹The School of Vehicle and Mobility, Tsinghua University, China

²The State Key Laboratory of Intelligent Green Vehicle and Mobility, Tsinghua University, China

³Sorbonne University, France

⁴Tencent Technology (Beijing) Co., Ltd

⁵University of Illinois at Urbana-Champaign, USA

*Corresponding author: Lei He (helei2023@tsinghua.edu.cn).

utilizes semantic labels to guide the generation of Gaussian ellipsoids. This method adaptively allocates computing resources according to the importance of Gaussian points. However, the methods above often suffer from increased rendering times and are sensitivity to regularization quality. Furthermore, these methods lack generalization capabilities across different scenes.

B. Feed-forward Networks for 3DGS

Recently, many feed-forward models for 3DGS [3, 4, 5, 6, 7, 9, 10] have emerged, aiming to directly predict Gaussian parameters to enhance scene reconstruction and reduce rendering time. PixelSplat [3, 29, 30] uses the transformer to encode image features and decode them into Gaussian parameters, addressing scale ambiguity but at high computational cost. SplatterNet [6] employs a U-Net model for object-level reconstruction from images, but its applicability to general scene-level reconstruction is limited. Different from these image-based methods, this paper explores an effective feed-forward model based on point cloud data. By learning from different kinds of scene point clouds, the proposed network can directly generate higher-quality initial Gaussian ellipsoids from sparse point clouds. Our approach not only enhances scene quality but also demonstrates strong generalization capabilities across various scenes.

III. METHOD

In the original 3D Gaussian Splatting (3DGS) method[2], the initial attributes of Gaussian ellipsoids are generated using heuristic methods from sparse SfM point clouds [31, 32]. This heuristic, scene-specific initialization strategy both limits the method’s generalization ability and overlooks the unique characteristics of different scenes. Additionally, it struggles to capture fine details in areas with insufficient texture due to the sparsity of input. These shortcomings result in decreased robustness when the model handles novel viewpoints or distant scenes.

To address these issues, we propose GS-Net, a generalizable, plug-and-play 3DGS module, as shown in Fig. 1. This network takes sparse point clouds as input and enhances cross-scene generalization and robustness. Taking specific characteristics of various scenes into consideration, GS-Net generates predicted dense ellipsoids that better represent scene features and reduce randomness.

A. Preliminary

3D Gaussian Splatting (3DGS) [2] uses innovative Gaussian primitives to represent a scene. A set of Gaussian primitives is represented as $\{g_n = (\mu_n, \Sigma_n, \alpha_n, C_{\text{rgb}_n})\}_M^n$ [3] with the definition for each one:

$$G(x_n) = e^{-\frac{1}{2}(x_n - \mu_n)^T \Sigma_n^{-1} (x_n - \mu_n)} \quad (1)$$

where μ_n refers to its mean vector, and Σ_n is its covariance matrix, which is decomposed into a rotation matrix R and scaling S , as $\Sigma_n = RSS^T R^T$. Besides, the opacity α_n , and color C_{rgb_n} computed by spherical harmonics (SH)

coefficients are defined for image rendering. The color of each pixel p of rendered image is computed:

$$C(p) = \sum_n C_{\text{rgb}_n} \alpha_n \prod_{j=1}^{n-1} (1 - \alpha_n) \quad (2)$$

The quality of Gaussian primitives directly affects the effectiveness of scene reconstruction. However, during the initial stage of 3DGS, if the point cloud is too sparse, artifacts may arise in the optimization of ellipsoids due to insufficient supervision [15]. Our experiments demonstrate that when the quality of the initial ellipsoids is high, the final rendering performance of 3DGS can be significantly improved. Moreover, achieving a generalized initialization for different scenes is crucial for improving efficiency [3]. Our goal is to address these issues.

B. Initial Parameter Definitions

In this section, we introduce the fundamental parameters used in GS-Net, including sparse point clouds and predicted ellipsoid arrays, as well as dense point clouds and dense ellipsoid arrays. The former refers to the input and output of our model, while the latter is used to construct the ground truth for training.

Sparse SfM Point Cloud The SfM Point Cloud is obtained through the Structure from Motion technique [15]. The information contained in the point cloud is $\{sp_n = (p_n, C_{\text{rgb}_n})\}_N^n$, where p_n represents the 3D coordinates of the point (x, y, z) , and C_{rgb_n} represents the color of the point.

Dense Point Cloud The dense point cloud is obtained through the Multi-View Stereo (MVS) method [16], and we represent it as $\{dp_n = (p_n, C_{\text{rgb}_n})\}_D^n$.

Dense Ellipsoid Array The above dense point cloud is input into 3DGS to generate the dense ellipsoid array. Compared to sparse point cloud, this kind of input can result in a higher-quality dense ellipsoid array [17], which is used to construct our ground truth for network training. We represent the dense ellipsoid array as $\{g_n = (\mu_n, \Sigma_n, \alpha_n, C_{\text{rgb}_n})\}_D^n$.

Predicted Ellipsoid Array: After network prediction, we obtain the Predicted Ellipsoid Array, represented as $\{g_n = (\mu_n, \Sigma_n, \alpha_n, C_{\text{rgb}_n})\}_{T*N}^n$. Our network increases the density of the input by a factor of T , where T is a hyperparameter. On our dataset, we’ve selected $T = 5$ to achieve optimal densification. Each predicted ellipsoid has 14-dimensional attributes: μ_n (1×3), Σ_n (1×7), α_n (1×1), and C_{rgb_n} (1×3).

C. Network Model

As mentioned earlier, our GS-Net is applied to generate higher-quality initial Gaussian ellipsoids, replacing the original process of 3DGS and enhancing the ability to generalize across different scenes. As depicted in Fig. 1, the model’s input is the sparse point cloud, reconstructed using COLMAP[15], and the output is the predicted dense ellipsoid array. Next, we will introduce the components of our model, including the encoder, the decoder, and the activation functions applied to different Gaussian primitives.

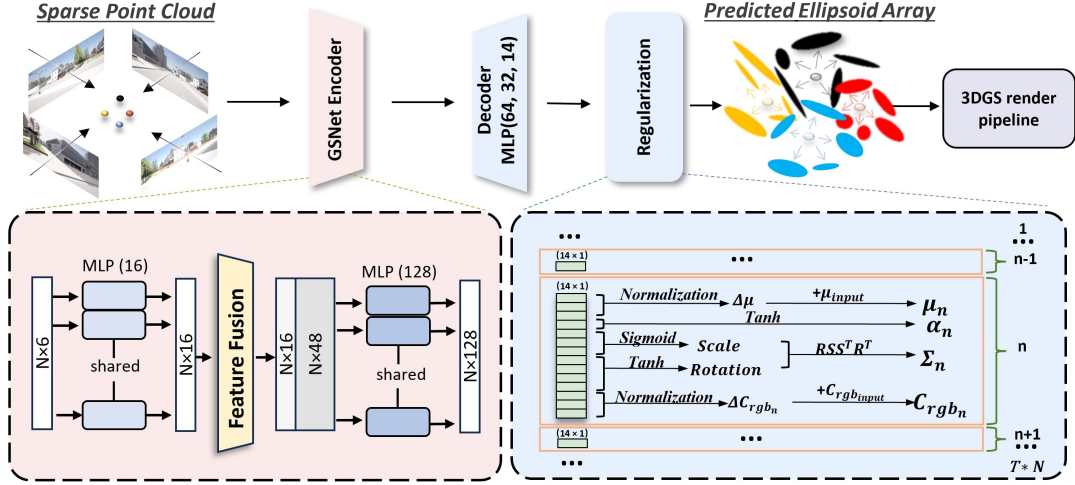


Fig. 1: The pipeline of GS-Net. We take sparse point clouds as input and output the predicted dense ellipsoid array. Each point of the input generates T Gaussian ellipsoids, which allows for higher quality and denser representation of local scenes. The light colored arrows on *Predicted Ellipsoid Array* image indicate this generation.

GS-Net Encoding Module The encoding module includes feature extraction and feature fusion for capturing essential point-wise and local features respectively. In detail, the first feature extraction module takes point position μ and color c_{rgb} as input (6-dimension) and outputs 16-dimensional features. Then, the feature fusion module finds the 3 nearest neighbors for each point and concatenates their features, forming a 64-dimensional feature vector (16×4). Finally, we use other feature extraction to further fuse neighbor features, ultimately generating 128-dimensional features, which are the output of our encoder. By incorporating neighborhood information, the model can represent the geometric structure of the scene more effectively[18], making the predicted ellipsoids more accurate. This design also equips GS-Net with the ability to adapt to various scene types. The overall process of the encoder can be found in Fig. 1.

Decoder As shown in Fig. 1, the decoder processes the output from the encoder through three fully connected layers, gradually reducing dimensions from 128 to a final 14-dimensional output, matching the dimensions required for the Predicted Ellipsoid Array.

Before obtaining the final output, we apply various regularization methods to each set of parameters in the Predicted Ellipsoid Array $g_n = (\mu_n, \Sigma_n, \alpha_n, C_{rgb_n})_{T \times N}^n$ to enhance the accuracy and convergence of the model predictions.

Opacity α : We regularize the opacity α using the Tanh [19] activation function. This ensures that the output values fall within the range of $[-1, 1]$.

Covariance Matrix Σ : The covariance matrix is composed of 3-dimensional scales and rotations (quaternion).

- **Scale:** The Sigmoid [20] activation function regularizes the scale values, ensuring they remain within a reasonable range.
- **Rotation:** The quaternion is normalized [21] to ensure the validity of the rotation matrix.

Position μ : For position, we don't apply regularization but instead employ a learning approach based on relative offsets to infer the position of densified points. This method allows for more stable position predictions. Further details will be provided in the *V. EXPERIMENTS – D. Ablation* section.

Color C_{rgb} : For C_{rgb} color, we also learn the delta value ΔC_{rgb} to more accurately represent scene changes.

Loss Function Setup During training, we use MSE as loss function[22]. Both position and color use delta values, while others use absolute values. The loss function is:

$$\text{Loss} = \text{MSE}(\delta(\mu) + \delta(c_{rgb}) + \alpha + \Sigma) \quad (3)$$

Through the model design outlined above, we have obtained a predicted dense ellipsoid array that can effectively capture local features across multiple scenes. Our method is efficient yet simple, allowing for cross-scene generalization and achieving higher-quality initialization.

IV. DATASET CARLA-NVS

To comprehensively evaluate scene reconstruction quality and the performance of GS-Net in autonomous driving scenarios, we have constructed a custom dataset named **CARLA Autonomous Vehicle Scene Dataset with Novel Viewpoints(CARLA-NVS)** using the CARLA simulator, incorporating novel viewpoints. Current open-source, real-world autonomous driving datasets are limited by their fixed camera positions on vehicles, which restrict the evaluation of scene reconstruction from unseen perspectives (such as the 5 cameras used in Waymo[24] and the 6 cameras in nuScenes[23]). Therefore, our goal is to generate a dataset that integrates dynamic and static scenes with multi-views and multi-sensors comprehensively. This dataset offers novel free viewpoints, making it better suited for verifying model performance in novel view synthesis.

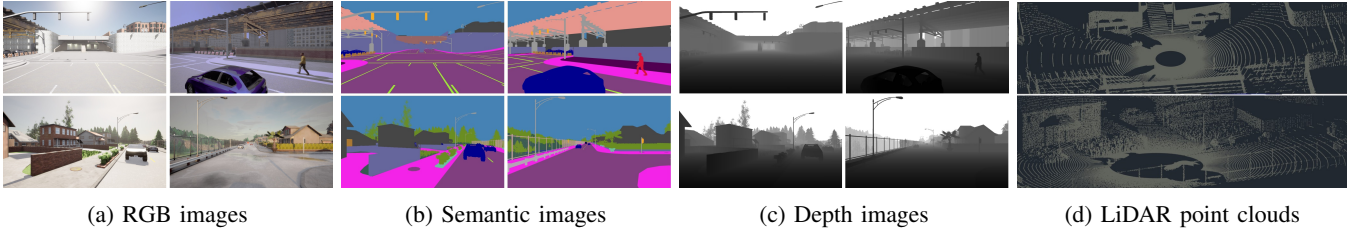


Fig. 2: Sample Examples of the CARLA-NVS Dataset. We showcase RGB, depth, semantic segmentation images, and LiDAR point clouds from two scenes under different viewpoints and weather conditions.

A. Scene Setup

The dataset covers various typical driving environments, including urban streets, rural roads, and highways. The dynamic scenes in CARLA-NVS are generated using CARLA’s path planning system and include moving vehicles, pedestrians, and bicycles, simulating complex traffic conditions. The static scenes contain only parked vehicles and fixed infrastructure (such as road signs, trees, and buildings), which are used in our experiments to evaluate reconstruction quality under static conditions. Additionally, all data is collected under two weather conditions, sunny and cloudy, further enhancing the diversity of the dataset.

B. Sensor Configuration

To ensure the diversity and richness of the CARLA-NVS dataset, we employ the following types of sensors in the scenes to collect multiple types of data:

- **RGB Camera Sensors:** Capture color images of the environment with a resolution of 1920x1080.
- **Depth Camera Sensors:** Provide depth information between the sensor and objects in the scene, with a resolution of 1920x1080.
- **Semantic Segmentation Camera Sensors:** Generate semantic labels for each pixel in the scene, with a resolution of 1920x1080.
- **LiDAR Sensors:** Provide a 360-degree LiDAR sensor that captures 3D point clouds with a maximum detection range of 200 meters and generates 3 million points per second with 128 scan channels.

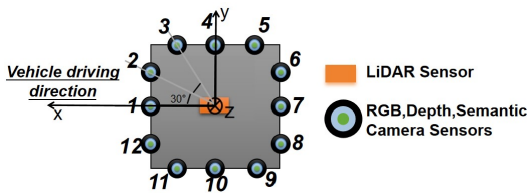


Fig. 3: Sensor configuration on the vehicle in the CARLA-NVS dataset.

As shown in Fig. 3, in conventional sensor setups, sensors are positioned at specific views, such as 1, 3, 5, 7, 9, and 11, leaving gaps between viewpoints. To improve coverage in our dataset, we add sensors at positions 2, 4, 6, 8, 10, and 12. As a result, the vehicle is equipped with twelve

RGB, depth, and semantic segmentation cameras, each with a 90-degree FOV, uniformly distributed at 30-degree intervals. Additionally, a LiDAR sensor is mounted at the top center of the vehicle to enhance 3D environmental mapping. Overall, this setup provides 360-degree coverage, enabling accurate evaluation from unseen perspectives. Notably, the dataset is designed not only for novel viewpoint evaluation in 3DGS, but also for the multiple autonomous driving tasks, such as BEV perception and Occupancy detection.

Based on the above definitions, we generate 20 scenes. Specifically, in each scene, data from all sensors are collected simultaneously at 10 Hz, lasting 10 seconds (approximately 100 meters of street driving), resulting in 100 frames of data per sensor. The data generated for each scene includes 1,200 RGB images, 1,200 depth images, 1,200 semantic segmentation images, and 30 million LiDAR point clouds, as shown in Fig. 2. The collected data are pre-processed to ensure uniformity and usability. All image data are stored in PNG format, while point cloud data is stored in PCD format. Each frame is timestamped to ensure precise alignment during subsequent analyses.

V. EXPERIMENTS

A. Dataset Preparation and Implementation Details

The CARLA-NVS dataset consists of 10 static and 10 dynamic scenes. In our experiments, we select the 10 static scenes and capture 100 seconds of RGB data using cameras 1, 3, 5, 7, 9, and 11. During training, we first select 90-second image sequences and use SfM[31, 32] and MVS [16] to generate dense point clouds, which are then input into 3DGS[2] to produce dense ellipsoid arrays as the ground truth for training. When testing, we use 10 different one-second image sequences across scenes to evaluate the performance of GS-Net. Two evaluation approaches are employed:

GS-Net+3DGS Under Conventional Viewpoints In this part, we use one-second image sequences captured by cameras 1, 3, 5, 7, 9, and 11, consisting of 60 images. We select 52 images as the working set (used for 3DGS optimization training), with the remaining 8 images reserve as testing views for final rendering evaluation. COLMAP[15] is used to reconstruct the point clouds from the working set, which are then input into GS-Net to generate dense Gaussian ellipsoids, serving as the initial ellipsoids for the optimization of 3DGS.

GS-Net+3DGS Under Novel Viewpoints In this part, we use one-second image sequences captured by 12 cameras,

totaling 120 images. We select 60 images from cameras 1, 3, 5, 7, 9, and 11 as the working set, while the remaining 60 images from cameras 2, 4, 6, 8, 10, and 12 are reserved as the testing set. The final rendering evaluations are conducted using the same approach as previously described for the working and testing sets.

To further validate the adaptability of GS-Net as a plug-and-play module, we apply it to GaussianPro [27]. GaussianPro takes sparse point clouds as input and applies a progressive propagation strategy to densify the Gaussian ellipsoids. In this evaluation, we first use GS-Net to predict dense Gaussian ellipsoids from the sparse input, and then follow GaussianPro’s training plan to assess the rendering quality under conventional viewpoints.

We use three standard evaluation metrics to assess performance: peak signal-to-noise ratio (PSNR), structural similarity index measure (SSIM), and learned perceptual image patch similarity (LPIPS) [26]. All experiments are conducted on a Tesla T4 GPU [25].

B. Training Strategy

This section introduces the distinctive training strategy of the model. We provide a detailed explanation of the input and ground truth construction, along with two key learning strategies.

Construction of Model Inputs and Ground Truth We use the sparse point clouds as input and derive the model’s ground truth from the dense ellipsoid array as mentioned in III. Method- B. *Initial Parameter Definitions*. Specifically, we construct a KDTree [33] using the centers μ_n of the dense ellipsoid array. For each sparse point s_n with position p_n , we find the five nearest ellipsoids in the dense ellipsoid array:

$$\{gd_{n_1}, gd_{n_2}, \dots, gd_{n_5}\} = \text{KDTree.query}(p_n, 5) \quad (4)$$

The parameters of these five nearest Gaussian ellipsoids (such as the mean μ , covariance matrix Σ , opacity α , and color C_{rgb}) are recorded as the ground truth.

Learning of Delta Values In the training process, we don’t directly learn the absolute position and color values between the input and the ground truth. Instead, we learn the delta values, which represent the offsets between them. Let the coordinates and color values of the input point be denoted as $\mathbf{p}_{\text{input}} = (x_i, y_i, z_i, r_i, g_i, b_i)$, and the target point coordinates and color values as $\mathbf{p}_{\text{target}}^{(i)} = (x_t^{(i)}, y_t^{(i)}, z_t^{(i)}, r_t^{(i)}, g_t^{(i)}, b_t^{(i)})$, where $i = 1, \dots, T$. Experiments have shown that learning delta values in this way improves model performance and is more effective than directly learning absolute values.

C. Quantitative and Qualitative Results

In this section, we evaluate the performance of GS-Net on the CARLA-NVS dataset within 3DGS [2] and its derivative method, GaussianPro [27]. Through comparisons with the original 3DGS method, we demonstrate that GS-Net achieves significant improvements across multiple evaluation metrics. On conventional viewpoints, GS-Net improves PSNR by 2.08 dB, and on novel viewpoints by 1.86 dB. Additionally,

when applied to GaussianPro, GS-Net also shows remarkable improvements, with a PSNR increase of 2.17 dB on conventional viewpoints. This indicates that GS-Net not only performs excellently within the original 3DGS method but also exhibits generalization capability and adaptability as a plug-and-play module. After GS-Net, the predicted denser initial ellipsoids can better capture the detailed features of the scene, resulting in higher-quality rendering in both textured and textureless regions, as shown in Fig. 4.

Results on GS-Net+3DGS under Conventional Viewpoints As shown in Fig. 4 and the first two rows of Table I, II and III, GS-Net significantly outperforms the original 3DGS across all evaluation metrics. In street scenes, regions with less prominent textures and depth information are difficult to accurately initialize through SfM point clouds, making it challenging for 3DGS to achieve precise Gaussian representation in these geometric areas. In contrast, our method generates dense and accurate ellipsoid information for these difficult-to-initialize regions, resulting in clearer and more accurate final rendering.

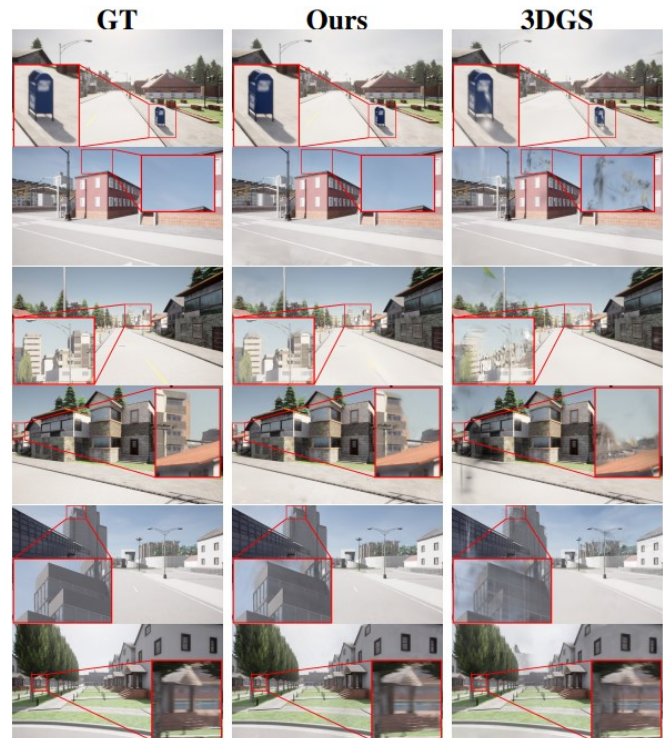


Fig. 4: Rendering results on the CARLA-NVS datasets. GS-Net achieves significant improvements over 3DGS, especially in rendering texture-less surfaces and fine details like lane markings.

Results on GS-Net+3DGS under Novel Viewpoints We train the model using conventional viewpoints and test it on novel viewpoints, where GS-Net also shows excellent performance. As shown in the first and third rows of Table I, II and III, the evaluation results of the original 3DGS on novel viewpoints are significantly lower than those on conventional viewpoints, primarily due to different camera

installation locations and changes in orientation. However, GS-Net generates more accurate ellipsoid information in supervised viewpoints and outperforms the original 3DGS even in the unsupervised viewpoints, as shown in the third and fourth rows of Table I, II and III. By achieving precise ellipsoid initialization, we improve the rendering quality of 3DGS in novel viewpoints.

Results on GS-Net+GaussianPro under Conventional Viewpoints GaussianPro, a derivative of the 3DGS method, also uses SfM point clouds as input. We apply our method to GaussianPro to evaluate the effectiveness of GS-Net as a plug-and-play network module. As shown in the fifth and sixth rows of Table I, II and III, the results show improvements across multiple evaluation metrics. These results demonstrate that our method provides better initial ellipsoids, allowing GaussianPro’s progressive propagation strategy to perform more effectively during the optimization process.

TABLE I: PSNR comparisons on the CARLA-NVS. The highest PSNR values under the same evaluation configuration are indicated in bold. *CV* represents conventional viewpoints, and *NV* represents novel viewpoints.

Method	Scene1	Scene2	Scene3	Scene4	Scene5
3DGS CV	26.80	27.36	27.95	24.35	24.66
GS-Net+3DGS CV (Ours)	29.62	28.43	30.06	28.08	25.32
3DGS NV	20.85	21.52	21.44	21.02	20.07
GS-Net+3DGS NV (Ours)	21.98	22.73	23.85	24.33	21.31
GaussianPro CV	26.91	27.52	28.21	24.61	24.76
GS-Net+GaussianPro CV (Ours)	29.27	29.19	30.56	28.35	25.22

TABLE II: SSIM comparisons on the CARLA-NVS.

Method	Scene1	Scene2	Scene3	Scene4	Scene5
3DGS CV	0.929	0.942	0.941	0.915	0.867
GS-Net+3DGS CV (Ours)	0.947	0.946	0.954	0.936	0.870
3DGS NV	0.855	0.870	0.873	0.865	0.798
GS-Net+3DGS NV (Ours)	0.862	0.871	0.875	0.869	0.800
GaussianPro CV	0.933	0.936	0.944	0.927	0.868
GS-Net+GaussianPro CV (Ours)	0.948	0.943	0.953	0.938	0.873

TABLE III: LPIPS comparisons on the CARLA-NVS.

Method	Scene1	Scene2	Scene3	Scene4	Scene5
3DGS CV	0.166	0.152	0.152	0.225	0.202
GS-Net+3DGS CV (Ours)	0.131	0.139	0.141	0.160	0.192
3DGS NV	0.233	0.227	0.252	0.311	0.335
GS-Net+3DGS NV (Ours)	0.213	0.216	0.245	0.241	0.330
GaussianPro CV	0.147	0.146	0.139	0.179	0.199
GS-Net+GaussianPro CV (Ours)	0.129	0.142	0.121	0.157	0.191

D. Ablation

We conduct extensive ablation experiments to validate the effectiveness of our model. Here, we mainly evaluate the impact of learning delta positions. With the input shown in Fig. 5a, the prediction of learning absolute values introduces a noticeable positional error, resulting in an enlargement of the scene, as shown in Fig. 5b. However, the result obtained by learning delta values in Fig. 5c shows great densification around the sparse point clouds.



(a) Sparse Point Cloud (b) Learn absolute values (c) Learn delta Values

Fig. 5: Visualization of Delta Learning Effects. (a) shows our sparse point cloud. (b) represents the output from learning absolute positions. (c) displays the output from learning delta positions, which adheres to the scene’s geometric structure and achieves densification.

E. Efficiency Analysis

We select two typical street scenes from the CARLA-NVS dataset to compare the performance of our method against using SfM or MVS point clouds as inputs to the 3DGS pipeline, as shown in Table IV. Compared to SfM+3DGS, our method achieves significantly better quality while slightly reducing the training time. While using dense MVS point clouds in 3DGS yields superior rendering results, it significantly increases the training time due to the extra processing and the larger number of initial Gaussians. In contrast, our method strikes a better balance between rendering quality and efficiency. Additionally, it does not require scene-specific MVS point clouds, enabling it to generalize across different scenes.

TABLE IV: Efficiency analysis comparing different initialization strategies with SfM points, MVS points, and GS-Net points. We indicate the best and second best with bold and underlined, respectively.

Scene	Strategy	PSNR	Training time
Scene 1	SfM points+3DGS	26.80	<u>62min</u>
	MVS points+3DGS	29.64	153min
	GS-Net+3DGS (ours)	<u>29.62</u>	58min
Scene 2	SfM points+3DGS	27.36	<u>77min</u>
	MVS points+3DGS	28.82	191min
	GS-Net+3DGS (ours)	<u>28.43</u>	71min

VI. CONCLUSIONS

This paper introduces GS-Net, a generalizable plug-and-play 3DGS module capable of cross-scenario rendering for autonomous driving, with strong feature extraction and geometric representation capabilities. As a plug-and-play solution, GS-Net demonstrates excellent practicality and compatibility with 3DGS and its derivatives. To evaluate its performance, we developed the CARLA-NVS dataset, supporting 12 camera viewpoints. Experimental results show that GS-Net significantly improves 3DGS rendering quality across both conventional and novel viewpoints, while maintaining comparable rendering speeds. Future work will focus on optimizing generalization and precision, with plans to release the CARLA-NVS dataset upon acceptance.

REFERENCES

- [1] G. Chen and W. Wang, “A survey on 3D Gaussian splatting,” *arXiv preprint arXiv:2401.03890*, 2024.
- [2] B. Kerbl, G. Kopanas, T. Leimkühler, and G. Drettakis, “3D Gaussian splatting for real-time radiance field rendering,” *ACM Trans. Graph.*, vol. 42, no. 4, pp. Art. no. 86, 19 pages, July 2023.
- [3] D. Charatan, S. Li, A. Tagliasacchi, and V. Sitzmann, “PixelSplat: 3D Gaussian splats from image pairs for scalable generalizable 3D reconstruction,” in *Proc. IEEE/CVF Conf. Comput. Vis. Pattern Recognit. (CVPR)*, 2024, pp. 1234–1243.
- [4] A. Chen, H. Xu, S. Esposito, S. Tang, and A. Geiger, “LARA: Efficient large-baseline radiance fields,” in *Proc. Eur. Conf. Comput. Vis. (ECCV)*, 2024, pp. 567–576.
- [5] S. Szymanowicz *et al.*, “Flash3D: Feed-forward generalisable 3D scene reconstruction from a single image,” *arXiv preprint arXiv:2406.04343*, 2024.
- [6] S. Szymanowicz, C. Rupprecht, and A. Vedaldi, “Splatter image: Ultra-fast single-view 3D reconstruction,” in *Proc. IEEE/CVF Conf. Comput. Vis. Pattern Recognit. (CVPR)*, 2024, pp. 2345–2354.
- [7] C. Wewer *et al.*, “LatentSplat: Autoencoding variational Gaussians for fast generalizable 3D reconstruction,” in *Proc. Eur. Conf. Comput. Vis. (ECCV)*, 2024, pp. 789–798.
- [8] Z. Zhu, Z. Fan, Y. Jiang, and Z. Wang, “FSGS: Real-time few-shot view synthesis using Gaussian splatting,” *arXiv preprint arXiv:2312.00451*, 2023.
- [9] K. Zhang, S. Bi, H. Tan, *et al.*, “GS-LRM: Large reconstruction model for 3D Gaussian splatting,” *arXiv preprint arXiv:2404.19702*, 2024.
- [10] S. Zheng *et al.*, “GPS-Gaussian: Generalizable pixel-wise 3D Gaussian splatting for real-time human novel view synthesis,” in *Proc. IEEE/CVF Conf. Comput. Vis. Pattern Recognit. (CVPR)*, 2024, pp. 3456–3465.
- [11] B. Xiong *et al.*, “SA-GS: Semantic-aware Gaussian splatting for large scene reconstruction with geometry constraint,” *arXiv preprint arXiv:2405.16923*, 2024.
- [12] B. Mildenhall *et al.*, “NeRF: Representing scenes as neural radiance fields for view synthesis,” in *Proc. Eur. Conf. Comput. Vis. (ECCV)*, 2020, pp. 405–421.
- [13] L. Chen *et al.*, “DeepDriving: Learning affordance for direct perception in autonomous driving,” *IEEE Trans. Intell. Transp. Syst.*, vol. 20, no. 5, pp. 1826–1836, 2019.
- [14] S. Zhu, R. Qin, G. Wang, J. Liu, and H. Wang, “SemGauss-SLAM: Dense semantic Gaussian splatting SLAM,” *arXiv preprint arXiv:2403.07494*, 2024.
- [15] J. L. Schönberger and J.-M. Frahm, “Structure-from-motion revisited,” in *Proc. IEEE Conf. Comput. Vis. Pattern Recognit. (CVPR)*, 2016, pp. 4104–4113.
- [16] Y. Furukawa and J. Ponce, “Accurate, dense, and robust multiview stereopsis,” *IEEE Trans. Pattern Anal. Mach. Intell.*, vol. 32, no. 8, pp. 1362–1376, 2010.
- [17] Z. Zhu *et al.*, “FSGS: Real-time few-shot view synthesis using Gaussian splatting,” *arXiv preprint arXiv:2312.00451*, 2023.
- [18] C. R. Qi *et al.*, “PointNet++: Deep hierarchical feature learning on point sets in a metric space,” in *Adv. Neural Inf. Process. Syst.*, vol. 30, 2017, pp. 5099–5108.
- [19] Y. LeCun *et al.*, “Efficient backprop,” in *Neural Networks: Tricks of the Trade*, G. Montavon, G. B. Orr, and K.-R. Müller, Eds. Springer, 2012, pp. 9–48.
- [20] X. Glorot, A. Bordes, and Y. Bengio, “Deep sparse rectifier neural networks,” in *Proc. 14th Int. Conf. Artif. Intell. Stat. (AISTATS)*, 2011, pp. 315–323.
- [21] Y.-B. Jia, “Quaternions and rotations,” *Com S 477/577 Notes*, Iowa State Univ., 2008, pp. 1–15.
- [22] C. M. Bishop, *Pattern Recognition and Machine Learning*. New York, NY, USA: Springer, 2006.
- [23] H. Caesar *et al.*, “nuScenes: A multimodal dataset for autonomous driving,” in *Proc. IEEE/CVF Conf. Comput. Vis. Pattern Recognit. (CVPR)*, 2020, pp. 11621–11631.
- [24] P. Sun *et al.*, “Scalability in perception for autonomous driving: Waymo Open Dataset,” in *Proc. IEEE/CVF Conf. Comput. Vis. Pattern Recognit. (CVPR)*, 2020, pp. 2446–2454.
- [25] NVIDIA Corporation, “Tesla T4 GPU architecture,” NVIDIA Corporation, Tech. Rep., 2018.
- [26] R. Zhang *et al.*, “The unreasonable effectiveness of deep features as a perceptual metric,” in *Proc. IEEE Conf. Comput. Vis. Pattern Recognit. (CVPR)*, 2018, pp. 586–595.
- [27] K. Cheng *et al.*, “GaussianPro: 3D Gaussian splatting with progressive propagation,” in *Proc. 41st Int. Conf. Mach. Learn. (ICML)*, 2024, pp. 123–132.
- [28] L. He, L. Li, W. Sun, *et al.*, “Neural radiance field in autonomous driving: A survey,” *arXiv preprint arXiv:2404.13816*, 2024.
- [29] L. He, G. Wang, and Z. Hu, “Learning depth from single images with deep neural network embedding focal length,” *IEEE Trans. Image Process.*, vol. 27, no. 9, pp. 4676–4689, 2018.
- [30] L. He, Q. Dong, and G. Wang, “Fast depth extraction from a single image,” *Int. J. Adv. Robot. Syst.*, vol. 13, no. 6, p. 1729881416663370, 2016.
- [31] S. Vijayanarasimhan *et al.*, “SfM-Net: Learning of structure and motion from video,” *arXiv preprint arXiv:1704.07804*, 2017.
- [32] M. Klodt and A. Vedaldi, “Supervising the new with the old: Learning SFM from SFM,” in *Proc. Eur. Conf. Comput. Vis. (ECCV)*, 2018, pp. 698–713.
- [33] J. L. Bentley, “Multidimensional binary search trees used for associative searching,” *Commun. ACM*, vol. 18, no. 9, pp. 509–517, 1975.